AIP | Applied Physics Letters

Combinatorial exploration of rare-earth-free permanent magnets: Magnetic and microstructural properties of Fe-Co-W thin films

T. R. Gao, Y. Q. Wu, S. Fackler, I. Kierzewski, Y. Zhang et al.

Citation: Appl. Phys. Lett. **102**, 022419 (2013); doi: 10.1063/1.4775581
View online: http://dx.doi.org/10.1063/1.4775581
View Table of Contents: http://apl.aip.org/resource/1/APPLAB/v102/i2
Published by the American Institute of Physics.

Combinatorial exploration of rare-earth-free permanent magnets: Magnetic and microstructural properties of Fe-Co-W thin films

T. R. Gao,[1] Y. Q. Wu,[2] S. Fackler,[1] I. Kierzewski,[1] Y. Zhang,[2] A. Mehta,[3] M. J. Kramer,[2,4] and I. Takeuchi[1,a)]

[1]*Department of Materials Science and Engineering, University of Maryland, College Park, Maryland 20742, USA*
[2]*Ames Laboratory, Iowa State University, Ames, Iowa 50011, USA*
[3]*Stanford Synchrotron Radiation Lightsource, SLAC National Accelerator Laboratory, Menlo Park, California 94025, USA*
[4]*Department of Materials Science and Engineering, Iowa State University, Ames, Iowa 50011, USA*

(Received 16 September 2012; accepted 17 December 2012; published online 18 January 2013)

We have investigated the magnetic and structural properties of Fe-Co-W films using a composition spread technique. From the magnetometry measurements, large magnetization (900 emu/cm^3) and enhanced perpendicular coercive fields (2–3 kOe) of low W concentration films were observed. The synchrotron diffraction results show a structural transition from a crystalline to an amorphous state and the crystallization onset increases with increasing W concentration. The SEM and TEM characterizations show that the films with low W concentrations have vertically standing platelet-like grain structures which is ascribed to the enhanced coercive fields. Magnetometry studies indicate that as the W concentration increases, microstructural change results in evolution of magnetization reversal mechanism. © *2013 American Institute of Physics*.
[http://dx.doi.org/10.1063/1.4775581]

Permanent magnets are ubiquitous in modern technologies, and they play important roles in generators, motors, speakers, and relays. Today's high performance permanent magnets contain at least one rare earth element such as Nd, Sm, Tb, or Pr.[1–3] However, rare-earth elements are increasingly rare and expensive, and alternative permanent magnet materials which do not contain rare-earth elements are needed by the industry.[4] We are using thin film composition spreads generated by ternary co-sputtering to search for rare-earth free permanent magnet materials. The large magnetic anisotropy and large coercivity are the prerequisites for permanent magnet applications. High Curie temperatures as well as high magnetizations are also required for permanent magnets. There have been reports which suggest that 5d elements such as W, Mo, Hf, and Zr can be used to induce large magnetocrystalline anisotropy in Fe and Co because 5d elements have large spin-orbit coupling and can lead to strong 3d-5d hybridization.[5–7] Moreover, the change of electronic structure of 3d elements due to the 5d elements doping may increase spin-orbit coupling,[8,9] thus affecting the magnetocrystalline anisotropy. In this work, we looked at the Fe-Co-W system as an initial investigation into 5d-element doped Fe-Co system to explore possible magnetic materials with enhanced coercive fields.

400-nm thick composition spread films of the Fe-Co-W alloy system were deposited using magnetron co-sputtering on 3-in. diameter Si wafers (with 200 nm thick thermally oxidized SiO_2 layer) at room temperature. The details of the composition spread deposition technique are described elsewhere.[10] A physical shadow mask is used to separate the composition spread film into a grid of 5 mm × 5 mm regions. The room-temperature deposited samples were then post-annealed in vacuum at various temperatures. The average composition of each thin film region patterned into 5 mm × 5 mm squares on the wafer is determined by wavelength dispersive spectroscopy (WDS). Following the annealing process, we use synchrotron x-ray diffraction to map the structural properties of the entire composition spread across the wafers. Some of the wafers are cut into small pieces to characterize the magnetic and microstructural properties by vibrating sample magnetometry (VSM) and transmission electron microscopy (TEM), respectively.

On one set of composition spread wafers, the W composition ranged from 0 at. % to 50 at. % (atomic percent concentration), and the atomic percent concentration of Fe and Co ranged from 10% to 90%. Synchrotron X-ray diffraction (at Beam line 11–3, Stanford Synchrotron Radiation Laboratory) was performed on three Fe-Co-W composition spread wafers. They were: (1) as deposited at room temperature, (2) deposited at room temperature then annealed at 600 °C, and (3) deposited at room temperature and then annealed at 700 °C. Fig. 1 shows representative X-ray diffraction spectra of selected composition Fe-Co-W films from a wafer annealed at 600 °C. Two main diffraction peaks are observed in the crystalline part of the film, and they are identified as Fe-Co BCC (110) and (200) reflections with the d-spacings of 2.0 and 1.5 Å, respectively. As seen in Fig. 1, for the films with W concentrations of 17.9% and 34.7%, the (110) diffraction peak is much wider than that of the films with W concentrations of 2.2% and 6.7%, and the diffraction intensity of such high W concentration films is much weaker compared to the intensity of the peak in low W concentration films. These observations clearly indicate that the Fe-Co-W films are crystalline for low W concentrations, and they tend to become nanocrystalline-like to amorphous with increasing W concentration. This is consistent with the fact that the

a)Electronic address: takeuchi@umd.edu.

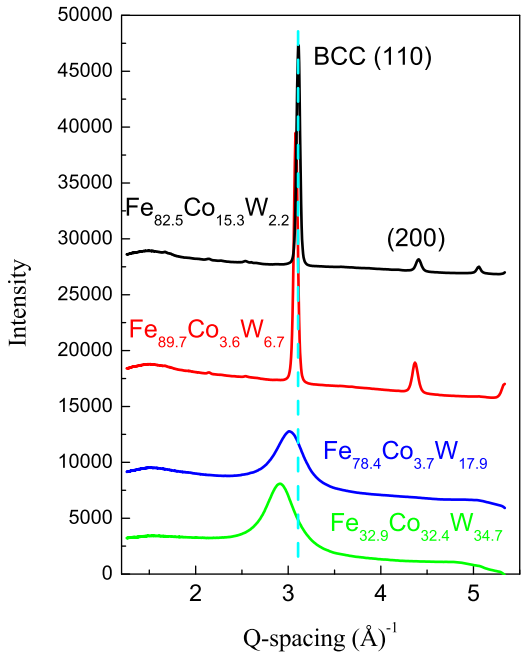

FIG. 1. Typical synchrotron XRD spectra of Fe-Co-W films annealed at 600 °C with various W contents.

crystallization temperature of W is substantially higher (1300–1500 °C) compared to that of Fe-Co, and thus material containing high concentration of W is less likely to form well-crystallized grains at annealing temperatures studied here. We also find that the d-spacing of the BCC (110) peak increases with increasing W concentration. This is an indication that despite the suppression of formation of a well-crystallized phase with increasing W concentration, W is indeed still being incorporated in the Fe-Co matrix: the increase in the d-spacing is due to the fact that the atomic radius of W (2.02 Å) is larger than that of Fe or Co (1.72 Å for Fe, and 1.67 Å for Co). Similar composition dependent structure trends were observed in the 700 °C annealed wafer.

In order to further elucidate the structural evolution from the amorphous-like to the crystalline state seen as a function of W concentration in Fe-Co-W, we have extracted the intensity and width (full width half maxima (FWHM)) of the BCC (110) diffraction peak from each diffraction spectrum on spread wafers. Fig. 2 shows the mapping of FWHM of the BCC (110) peak for the as-grown, 600 °C and 700 °C annealed composition spreads. As clearly seen in Fig. 2(b), the FWHM of the (110) peak for the 600 °C annealed wafer is much wider (denoted by the yellow or green dots) when the W content is above 15%, indicating the Fe-Co-W films are amorphous in this composition range. When the W concentration is lower than 15%, the FWHM is narrower, indicating a crystalline phase, represented by blue dots. The onset of crystallization of the amorphous phase fraction increases with increasing W concentration so that the transition occurs at 10% W for as-grown films (Fig. 2(a)), and increases to 20% for 700 °C annealed films (Fig. 2(c)). Thermodynamically equilibrated bulk alloys of Fe or Co have limited solubility of only a few at. % W.[11] The fact that there is a crystalline to amorphous transition as a function of the W concentration in our films is consistent with this limited solubility and the fast cooling rate of the sputtering process. The solubility limit is expected to increase with increasing temperature, resulting in the crystalline phase region extending into higher W concentrations as observed in Fig. 2. The presence of excess W which cannot go into the Fe-Co crystal lattice results in W segregating into a separate amorphous or disordered phase. The d-spacing map (not shown here) obtained from the XRD spectra for the spread samples shows the similar trend as a function of W concentration in that at the crystalline to amorphous transition, the primary scattering peak abruptly shifts from (110) BCC at $Q = 3.0\,\text{Å}^{-1}$ to a diffuse peak at $Q = 2.7\,\text{Å}^{-1}$.

To investigate detailed microstructural properties of Fe-Co-W, three samples with different W concentrations taken from a wafer annealed at 600 °C were analyzed by TEM. Fig. 3(a) shows a plane-view image and a selected area electron diffraction (SAED) pattern (inset) of a low W concentration film (2.2%). This film is completely crystallized based on SAED. The plan-view image reveals a platelet-like microstructure consisting of oriented nanograins approximately 150 nm in length and 25 nm in width, and the cross-sectional TEM (not shown here) shows that the platelet-like nanograins have a columnar feature. From the sharp diffraction rings in the SAED pattern, we identify the phase to have a BCC structure. Fig. 3(b) shows the planar TEM image and SAED of a region with high W concentration (17.9%). Such films can be classified as amorphous based on the halo-like rings seen in the SAED (inset). When the W concentration is as high as 30%, the bulk of the film appears completely amorphous but occasionally contain, micron-sized pure W grains. The TEM results are consistent with the synchrotron diffraction results represented in Figs. 1 and 2, where the films of low W concentrations show the BCC crystalline phase, and the films of high W concentrations show an amorphous state.

The room temperature magnetic hysteresis loops of the films were measured using VSM. Figs. 4(a) and 4(b) show the representative in-plane and out-of-plane M(H) loops of $Fe_{32.3}Co_{62.8}W_{5.9}$ and $Fe_{28.5}Co_{57.2}W_{14.3}$ films annealed at

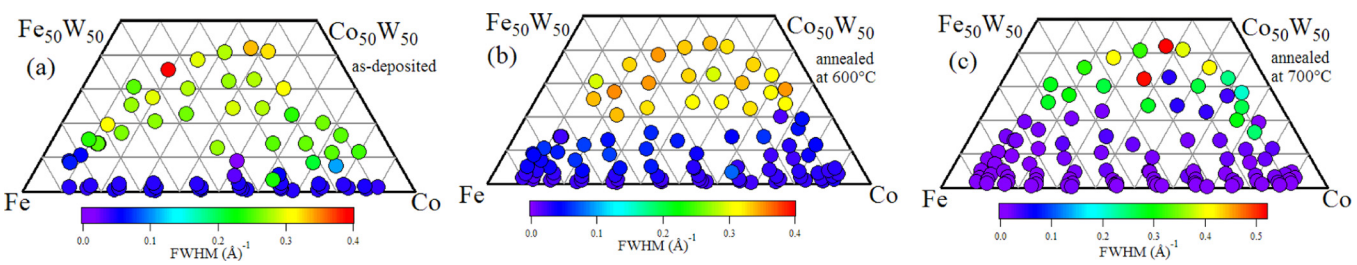

FIG. 2. FWHM spread in the composition library of Fe-Co-W films of as-deposited state (a) annealed at 600 °C (b) and annealed at 700 °C (c).

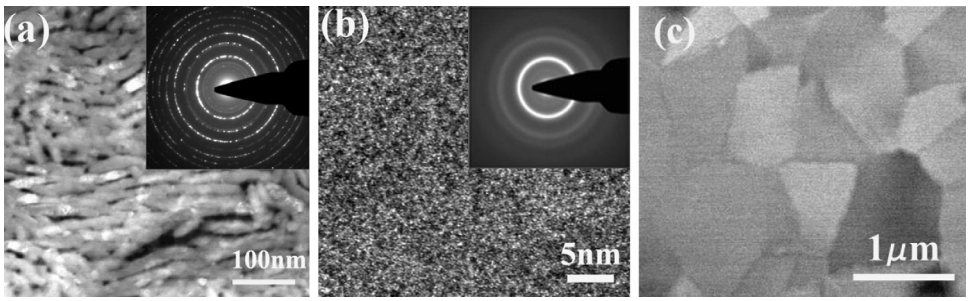

FIG. 3. TEM images of (a) crystallized region with 2.2% W concentrations with inset SAED demonstrating the crystalline state, (b) amorphous 17.9% W concentrations with inset SAED demonstrating the amorphous state, and (c) micron-sized crystalline W grains within the 34.7% W region which is primarily amorphous.

600 °C, respectively. As seen in Fig. 4(a), the out-of-plane coercivity of $Fe_{32.3}Co_{62.8}W_{5.9}$ is about 2.3 kOe indicating the presence of perpendicular anisotropy, although it is not fully saturated. Such a hysteresis loop with $H_c \sim$ 2-3 kOe was observed from many samples with similar compositions. The in-plane coercivity is small and shows a soft magnet-like characteristic with the saturation magnetization of 900 emu/cm^3, consistent with high moments of Fe and Co. The high W concentration films ($Fe_{28.5}Co_{57.2}W_{14.3}$) show magnetic single phase behavior, as seen in Fig. 4(b) where the out-of-plane coercivity is much smaller than that of low W concentration films. The saturation magnetization of 400 emu/cm^3 in the high W concentration film is much lower than 900 emu/cm^3 of low W concentration films. This is due to the fact that as the Fe-Co-W films become more and more amorphous-like with increasing W concentration, the material becomes less and less magnetic. When the average W concentration of the film is higher than 50%, the Fe-Co-W film shows a non-magnetic behavior.

The out-of-plane hysteresis loop of $Fe_{32.3}Co_{62.8}W_{5.9}$ (Fig. 4(a)) is indicative of the presence of two magnetic phases in this low W concentration region of the sample. One is the soft phase with in-plane magnetization which has the slope in the out-of-plane hysteresis due to its demagnetizing field, and we attribute this to the host matrix of the material in which the platelet-like nanograins reside. The other is

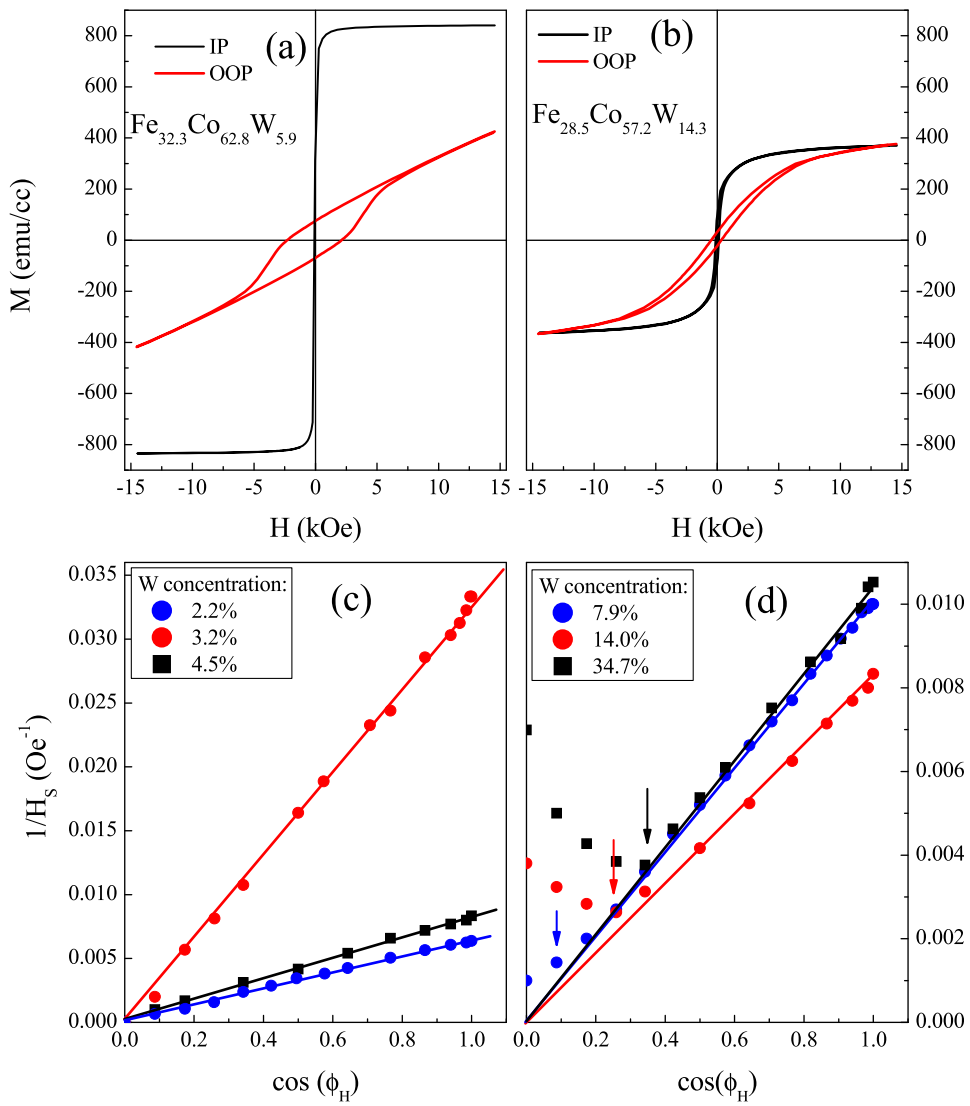

FIG. 4. Typical out-of-plane and in plane hysteresis loops of low W concentrations (a) and high W concentrations (b), and angular dependence of inverse H_S for low W concentrations (c), and high W concentrations (d). In (a) and (b), the IP and OOP denote the in-plane and out-of-plane M(H) loop with the magnetic field parallel and perpendicular to the film, respectively. In (c) and (d), the inset numbers refer to the W composition. The solid lines are from a linear fit. The arrows indicate the onset of the $\cos(\phi_H)$ for the inverse H_S to deviate from the linear dependence.

the hard phase with an enhanced coercivity (seen in the center of the curve) with large perpendicular magnetic anisotropy: this is from the platelet-like nanograins. This hard phase is not seen in the in-plane magnetic measurement since its volume fraction is presumably small compared to that of the soft matrix phase. Moreover, the out-of-plane hysteresis loops in Figs. 4(a) and 4(b) show a similar value of the slope (dM/dH), indicating that the soft magnetic part in both films has the similar demagnetization behavior. This further demonstrates that the linear part of out-of-plane hysteresis loop (displaying a two-phase behavior) comes from the soft host matrix in the low W concentration film (Fig. 4(a)).

We believe that the enhanced coercivity and the large perpendicular anisotropy mainly arise from the large demagnetization effect resulting from the large aspect ratio of the platelet-like nanograins seen in the TEM images. It is difficult to determine the magnetization of this hard phase due to the uncertainty in the exact relative volume fraction ration between the platelet-like hard phase and the soft host matrix. If we take, for instance, $M_s = 400\,\mathrm{emu/cm^3}$ for this hard phase, the demagnetization field for the platelet-like nanograins comes out to be $2\pi M_S \approx 2500$ Oe, and the shape anisotropy constant is $k_{shape} = 2\pi M_S^2 = 7 \times 10^5\,\mathrm{J\,m^{-3}}$, which is of the same order as the magnetocrystalline anisotropy of Co-Pt alloy.[12] This demagnetizing field of 2500 Oe is consistent with the observed saturation field of the hard-phase region of the out-of-plane hysteresis loop (central part of the loop).

It is instructive to investigate the magnetization reversal mechanism (MRM) of Fe-Co-W samples of different W concentrations since their microstructures are different for various compositions. In general, in magnetic films, the MRM can be described by three different modes, namely, (1) the pinning and motion of domain wall, (2) coherent rotation, and (3) coexistence of domain wall motion and coherent rotation, i.e., the Kondorsky model.[13] The MRM can be determined by the angular dependent switching field, H_S,[14,15] where H_S refers to the magnetic field which overcomes the irreversible motion of the domain wall. From the hysteresis loops at various applied field angle ϕ_H from in-plane to out-of-plane, the angular dependence of the switching field can be obtained, where ϕ_H is the angle between the plane of the film and that of the applied field. In order to delineate the relationship between H_S and ϕ_H clearly, we plot the inverse H_S as a function of $\cos(\phi_H)$ as shown in the Figs. 4(c) and 4(d). From Fig. 4(c), it is clear that the $1/H_s$ is proportional to $\cos(\phi_H)$ in the entire ϕ_H range from 0° to 90° when the W concentration is 2.2%, 3.2%, and 4.5%. This indicates that the MRM at these compositions is dominated by domain wall motion. For higher W concentration compositions (7.9%, 14.2%, and 34.7%), the $1/H_s$ is proportional to $\cos(\phi_H)$ only in a fixed range of ϕ_H, as indicated by arrows in Fig. 4(d): they obey domain wall motion for $\phi_H = 85°$, $\phi_H = 75°$, and $\phi_H = 70°$ for 7.9%, 14.2%, and 34.7% of W concentration samples, respectively. For larger angles, the MRM is dominated by the Kondorsky model, where domain wall motion and coherent rotation appear to coexist.

We believe the magnetization reversal mechanism is correlated with the microstructure of the films. For the platelet-like grain films, i.e., the low W concentration films, the effective anisotropy field H_k is expected to be larger than the pinning field H_p due to the large shape anisotropy of such standing grains, and the magnetization reversal process is dominated by domain wall displacement. However, for the higher W concentration samples where the coercivity is lower, the magnetic grains are embedded in amorphous matrix where their magnetizations switch separately, and therefore, the MRM is achieved by coherent rotation and domain wall motion.

In conclusion, the microstructural and magnetic properties of Fe-Co-W combinatorial films have been investigated by synchrotron X-ray diffraction, electron microscopy, and vibrating sample magnetometry. The microstructural characterization indicates that there exists a structural transition from crystalline to amorphous-like phases with increasing W concentration, and the onset of this crystallization increases with increasing W content. Enhanced perpendicular coercivity as large as 2.3 kOe is achieved at low W concentration. We believe this is mostly due to the shape anisotropy of platelet-like grains. We are currently investigating the growth mechanism of Fe-Co which leads to the platelet grain growth with incorporation of W. If it is possible to further engineer and control such grain growth, in principle, one can potentially achieve even larger coercive field due to their shape anisotropy. Fe-Co-W may be a potential rare-earth free permanent magnets candidate.

This work was funded by the beyond rare-earth permanent magnet project by the U.S. Department of Energy, Office of Energy Efficiency and Renewable Energy (EERE), under its Vehicle Technologies Program.

[1]J. M. D. Coey, *Rare-earth Iron Permanent Magnets* (Oxford University Press, Oxford, 1996).
[2]N. M. Dempsey, A. Walther, F. May, D. Givord, K. Khlopkov, and O. Gutfleisch, Appl. Phys. Lett. **90**, 092509 (2007).
[3]R. Skomski and J. M. D. Coey, *Permanent Magnetism* (Institute of Physics, London, UK, 1999).
[4]M. J. Kramer, R. W. McCallum, I. A. Anderson, and S. Onstantinides, JOM **64**, 752 (2012).
[5]S. M. Dubiel and W. Zinn, Phys. Rev. B **30**, 3783 (1984).
[6]N. Kikuchi, O. Kitakami, S. Okamoto, Y. Shimada, A. Sakuma, Y. Otani, and K. Fukamichi, J. Phys.: Condens. Matter **11**, L485 (1999).
[7]K. Kumasaka and K. Ono, J. Jpn. Inst. Met. **45**, 82 (1981).
[8]A. Kashya, P. Manchanda, P. K. Sahota, R. Skomski, J. E. Shield, and D. J. Sellmyer, IEEE Trans. Magn. **47**, 3336 (2011).
[9]H. Ebert, R. Zeller, B. Drittler, and P. H. Dederichs, J. Appl. Phys. **67**, 4576 (1990).
[10]I. Takeuchi, O. O. Famodu, J. C. Read, M. A. Aronova, K. S. Chang, C. Craciunescu, S. E. Lofland, M. Wuttig, F. C. Wellstood, L. Knauss, and A. Orozco, Nature Mater. **2**, 180 (2003).
[11]M. Lu and C. L. Chien, J. Appl. Phys. **67**, 5787 (1990).
[12]D. Weller, H. Brindle, G. Gorman, C. J. Lin, and H. Notarys, Appl. Phys. Lett. **61**, 2726 (1992).
[13]D. V. Ratnam and W. R. Buessem, J. Appl. Phys. **43**, 1291 (1972).
[14]T. R. Gao, S. P. Hao, S. M. Zhou, and L. Sun, J. Appl. Phys. **100**, 073909 (2006).
[15]X. X. Liu, Y. Shiozaki, and A. Morisako, J. Appl. Phys. **103**, 07E104 (2008).